INORGANIC CHEMISTRY

FRONTIERS

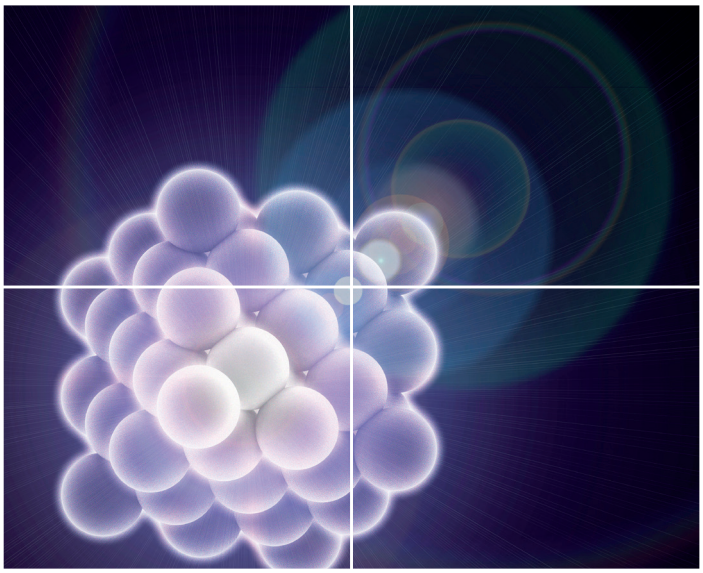

Accepted Manuscript

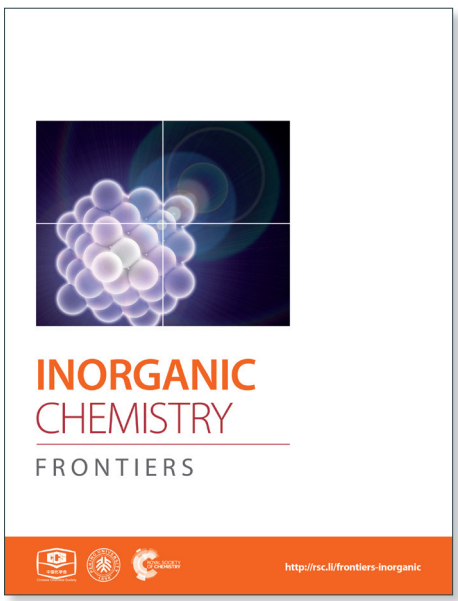

This is an *Accepted Manuscript*, which has been through the Royal Society of Chemistry peer review process and has been accepted for publication.

Accepted Manuscripts are published online shortly after acceptance, before technical editing, formatting and proof reading. Using this free service, authors can make their results available to the community, in citable form, before we publish the edited article. We will replace this *Accepted Manuscript* with the edited and formatted *Advance Article* as soon as it is available.

You can find more information about *Accepted Manuscripts* in the **Information for Authors**.

Please note that technical editing may introduce minor changes to the text and/or graphics, which may alter content. The journal's standard **Terms & Conditions** and the **Ethical guidelines** still apply. In no event shall the Royal Society of Chemistry be held responsible for any errors or omissions in this *Accepted Manuscript* or any consequences arising from the use of any information it contains.

Amide-containing zinc(II) metal–organic layer networks: structure–CO_2 capture relationship

Cheng-Hua Lee,[ab] Jing-Yun Wu,*[c] Gene-Hsiang Lee,[d] Shie-Ming Peng,[d] Jyh-Chiang Jiang,[e] and Kuang-Lieh Lu*[a]

[a]*Institute of Chemistry, Academia Sinica, Taipei 115, Taiwan. Fax: +886-2-27831237; E-mail: kllu@gate.sinica.edu.tw*

[b]*Graduate Institute of Applied Science and Technology, National Taiwan University of Science and Technology, Taipei 106, Taiwan*

[c]*Department of Applied Chemistry, National Chi Nan University, Nantou 545, Taiwan. E-mail: jyunwu@ncnu.edu.tw*

[d]*Department of Chemistry, National Taiwan University, Taipei 107, Taiwan*

[e]*Department of Chemical Engineering, National Taiwan University of Science and Technology, Taipei 106, Taiwan*

† Electronic Supplementary Information (ESI) available: [PXRD patterns, additional structure diagrams, CO_2 adsorption isotherms and hydrogen-bond parameters. CCDC reference number 1029622–1029623].

The self-assembly of zinc–organic coordination polymers $[Zn_2(1,3\text{-bdc})_2(bpda)_2]\cdot 3DMF\cdot 0.5H_2O$ (**1**, 1,3-bdc = 1,3-benzenedicarboxylate; bpda = *N,N′*-bis(pyridine-4-yl)-1,4-benzenedicarboxamide) and $[Zn_2(1,4\text{-ndc})(dmc)_2(bpda)_2]$ (**2**, 1,4-ndc = 1,4-naphthalenedicarboxylate; dmc = dimethylcarbamate) through mixed-ligand coordination under hydro(solvo)thermal conditions is reported. Both compounds **1** and **2** are made up of a two-dimensional layer network with a decorated 4^4-**sql** topology from the associated dinuclear two-blade paddlewheel building units. The bis-amide groups of the bpda ligands in the layered structures **1** and **2** are sheltered and participate in multiple hydrogen-bonding interactions. Compounds **1** and **2** are both high thermally stable at temperatures over 300 ℃ and exhibit solid-state luminescence properties. In comparison with the CO_2 adsorption behavior of the related compound $\{[Zn_4(1,4\text{-bdc})_4(bpda)_4]\cdot 5DMF\cdot 3H_2O\}_n$ (**3,** 1,4-bdc = 1,4-benzenedicarboxylate), the desolvated sample of **1** and the thermally-activated sample of **2** both show a lower CO_2 uptake capacity and a decreased Q_{st} trace with increasing CO_2 uptake. These results show that no meaningful cooperative binding occurs between the amide groups and CO_2 molecules in the condensed 2D structures of **1** and **2**. By varying the dicarboxylate ligand from 1,3-bdc, 1,4-ndc, to 1,4-bdc, the amide-functionalized products **1**–**3** induce subtle changes in their structures. In particular, the intimate interrelationship between the structural characteristics of amide groups and the CO_2 adsorption behavior of such compounds is clearly demonstrated.

Introduction

The design and construction of metal–organic frameworks (MOFs) has become a rapidly growing field in metal-based supramolecular chemistry and has triggered vigorous investigations in recent decades due to their potential in a range of achievable applications.[1–10] Porous MOFs have currently been developed for use as materials for use in capturing CO_2.[7–11] Further modification of internal cavities of such frameworks and an understanding of the interrelationship between their structural characteristics and CO_2 adsorption capability would be highly desirable.[8–11]

We recently reported on a unique CO_2 adsorption behavior of an amide-containing MOF.[11] A two-fold interpenetrated MOF $\{[Zn_4(1,4\text{-bdc})_4(bpda)_4]\cdot 5DMF\cdot 3H_2O\}_n$ (**3**, where 1,4-bdc = 1,4-benzene dicarboxylate, bpda = *N,N′*-bis(pyridine-4-yl)-1,4-benzenedicarboxamide) showed interesting characteristics, in which the unsheltered amide groups inside the open-ended channels cooperatively bind CO_2 molecules by not only amide:CO_2 binding but also amide:CO_2:CO_2 binding. These interactions result in a high isosteric heat of CO_2 adsorption (Q_{st}), which increases significantly with increasing CO_2 uptake. To further advance this ongoing project,[11,12] we envisaged that the replacement of other similar dicarboxylate bridging ligands such as 1,3-bdc (1,3-benzenedicarboxylate) and 1,4-ndc (1,4-naphthalenedicarboxylate) might significantly alter the special arrangement of the amide groups, thereby affecting their CO_2 adsorption behavior. Herein we report on the structures and CO_2 adsorption capabilities of a series of 1,3-bdc, 1,4-ndc and 1,4-bdc containing Zn(II) MOFs. An intimate interrelationship between the structural characteristics of their amide groups and CO_2 sorption behavior is observed and described.

Experimental section

Materials and general characterization

Ligand *N,N′*-bis(pyridine-4-yl)-1,4-benzenedicarboxamide (bpda) was prepared according to the literature method.[11] All other solvents and chemical reagents were purchased commercially and used as received without further purification. Infrared (IR) samples were prepared as KBr pellets, and spectra were obtained in the 4000–400 cm^{-1} range using a Perkin-Elmer Paragon 1000 FT-IR spectrophotometer; abbreviations used for the IR bands are w = weak, m = medium, s = strong. Elemental analyses were performed on a Perkin-Elmer 2400 CHN elemental analyzer. A Perkin-Elmer TGA-7 analyzer was used to carry out the thermogravimetric (TG) analysis under flowing nitrogen at a heating rate of 10 ℃ min^{-1}. Powder X-ray diffraction (PXRD) measurements were recorded on a Siemens D-5000 diffractometer at 40 kV, 30 mA for Cu Kα (λ = 1.5406 Å), with a

step size of 0.02° in θ and a scan speed of 1 sec per step size. The solid-state emission spectra were investigated with a Hitachi F-7000 Fluorescence Spectrophotometer at room temperature.

Synthesis of $[Zn_2(1,3\text{-bdc})_2(bpda)_2]\cdot 3DMF\cdot 0.5H_2O$ (1)

$ZnCl_2$ (13.7 mg, 0.10 mmol), 1,3-benzenedicarboxylic acid (1,3-H_2bdc, 16.8 mg, 0.10 mmol), bpda (31.9 mg, 0.10 mmol), DMF (7 mL), and H_2O (0.5 mL) were sealed in a Teflon-lined stainless steel Parr acid digestion bomb and heated at 100 ℃ for 72 h, which was then allowed to slowly cool to 30 ℃. Colorless block-shaped crystals were collected by filtration, washed with water, and dried in air. Yield: 51%. Elemental analysis calcd. for **1** ($C_{61}H_{58}N_{11}O_{15.5}Zn_2$): C, 55.34; H, 4.42; N, 11.64%. Found: C, 55.11; H, 4.61; N, 11.43%. IR (KBr pellet, cm^{-1}): 3455 (w), 3259 (w), 3176 (w), 3085 (w), 2928 (w), 1682 (s), 1598 (s), 1562 (w), 1498 (m), 1442 (w), 1422 (m), 1391 (s), 1330 (m), 1297 (m), 1261 (w), 1211 (m), 1116 (w), 1098 (m), 1076 (w), 1019 (m), 956 (w), 835 (m), 750 (m), 715 (m), 658 (w), 604 (w), 575 (w), 537 (m).

Synthesis of $[Zn_2(1,4\text{-ndc})(dmc)_2(bpda)_2]$ (2)

$ZnCl_2$ (13.6 mg, 0.10 mmol), 1,4-naphthalenedicarboxylic acid (1,4-H_2ndc, 21.9 mg, 0.10 mmol), bpda (32.0 mg, 0.10 mmol), DMF (7 mL), and H_2O (0.5 mL) were sealed in a Teflon-lined stainless steel Parr acid digestion bomb and heated at 120 ℃ for 96 h, which was then allowed to slowly cooled to 30 ℃. Colorless block-shaped crystals were collected by filtration, washed with water, and dried in air. Yield: 50%. Elemental analysis calcd. for **2** ($C_{54}H_{44}N_{10}O_{12}Zn_2$): C, 56.12; H, 3.83; N, 12.12%. Found: C, 56.23; H, 3.87; N, 12.23%. IR (KBr pellet, cm^{-1}): 3259 (w), 3174 (w), 3076 (w), 2926 (w), 2860 (w), 1686 (s), 1596 (s), 1568 (s), 1511 (s), 1422 (m), 1393 (w), 1370 (m), 1329 (s), 1299 (m), 1264 (m), 1210 (s), 1112 (m), 1098 (m), 1061 (w), 1019 (s), 835 (s), 797 (m), 770 (w), 736 (w), 711 (m), 661 (m), 603 (m), 565 (m), 537 (s).

Crystal data collection and refinement

Single-crystal X-ray diffraction analyses for **1** and **2** were performed on a Nonius KappaCCD diffractometer, equipped with graphite monochromatized Mo Kα radiation (λ = 0.71073 Å). Intensity data were collected within the limits of 1.04° ≤ θ ≤ 27.50° at 150(2) K for **1** and of 1.87° ≤ θ ≤ 26.37° at 100(2) K for **2**. The crystal structures were solved with the direct methods and refined with a full-matrix least-squares procedure on F^2 using the SHELX-97 program package.[13] Nonhydrogen atoms were found from the difference Fourier maps and most of them were treated anisotropically except where noted. In **1**, one pyridine ring of the bpda ligand was treated disorderedly over two occupied sites with equal refined site occupancy factors. All of the lattice DMF and H_2O molecules were refined isotropically, where some of them were treated disorderedly. Whenever possible, the hydrogen atoms were located on a difference Fourier map and refined. In other cases, the hydrogen atoms were geometrically fixed. Experimental details for X-ray data collection and the refinements are summarized in Table S1. CCDC 1029622 and 1029623 contain the supplementary crystallographic data for this paper. These data can be obtained free of charge from the Cambridge Crystallographic Data Centre via www.ccdc.cam.ac.uk/data_request/cif.

Low-pressure adsorption measurements

An ASAP 2020 Accelerated Surface Area and Porosimetry analyzer from Micrometrics was used to perform low-pressure carbon dioxide (CO_2) adsorption measurements. Research grade CO_2 (99.9995% purity) was used in all adsorption measurements. The materials were degassed prior to analysis. Fresh samples were loaded into a sample tube of known weight and activated at 120 ℃ under a high vacuum for about 24 h to completely remove guest solvent molecules. After activation, the sample and tube were re-weighed to determine the precise mass of the evacuated sample. CO_2 adsorption isotherms were measured at 195 K, 273 K, and 298 K.

Results and discussion

Synthesis and general characterization

Compound **1** was prepared by reacting $ZnCl_2$, bpda, and 1,3-H_2bdc in a DMF/H_2O solution under hydro(solvo)thermal conditions through a single-step self-assembly process, whereas compound **2** was prepared by a synthetic procedure similar to that used for **1**, using 1,4-H_2ndc instead of 1,3-H_2bdc (Scheme 1). Single-crystal X-ray diffraction analyses were carried out to determine the crystal structures of **1** and **2**. Powder X-ray diffraction (PXRD) patterns measured with the bulk materials of **1** and **2** confirm the phase purity of both materials (Figs. S1 and S2).

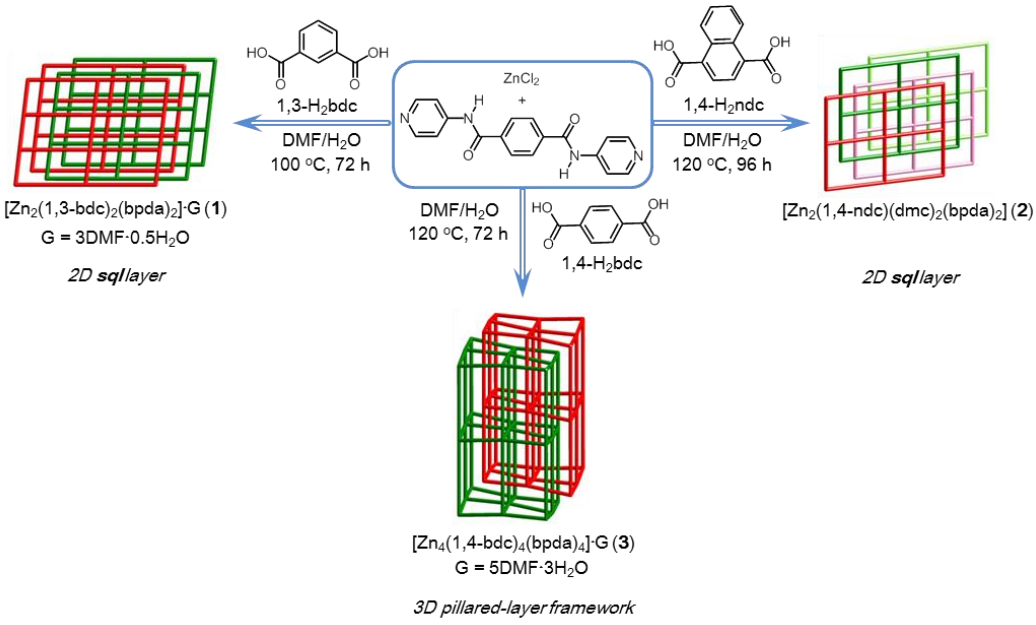

Scheme 1

Crystal structure description

$[Zn_2(1,3\text{-bdc})_2(bpda)_2]\cdot 3DMF\cdot 0.5H_2O$ (1)

A single-crystal X-ray diffraction analysis revealed that compound **1** crystallizes in the triclinic space group $P\bar{1}$. The asymmetric unit consists of two Zn(II) centers, two 1,3-bdc^{2-} and two bpda ligands, and a total of three lattice DMF and half of a lattice water molecules. Both the two crystallographically distinct Zn(II) centers adopt a five-coordinated $\{ZnN_2O_3\}$ trigonal bipyramidal geometry (Fig. 1a), with τ values of 0.89 and 0.87,[14] surrounded by two pyridine nitrogens of two different bpda ligands at the axial positions and three carboxyl oxygens of three different 1,3-bdc^{2-} ligands at the equatorial plane. The Zn−N bond lengths are in the range of 2.142(3)−2.165(3) Å, and the Zn−O bond lengths are in the range of 2.008(3)−2.045(3) Å. Each 1,3-bdc^{2-} ligand bridges three Zn(II) centers with one carboxyl group in a μ_2-η^1:η^1-bridging bidentate coordination mode and another in a monodentate mode. It should be noted that the remaining oxygen of the monodentate carboxylate group also interacts weakly with the Zn(II) center (Zn···O, 2.59 and 2.65 Å).

Two Zn(II) centers are held together by two carboxyl groups from two 1,3-bdc^{2-} ligands, thus forming a dinuclear $[Zn_2(CO_2)_4N_4]$ secondary building unit (SBU) with a Zn···Zn separation of 4.03 Å, which resembles a two-bladed paddlewheel (Fig. 1a). The SBUs are connected to each other by 1,3-bdc^{2-} ligands to generate a neutral one-dimemsional (1D) Zn–1,3-bdc chain array, which is then linked by pairs of bpda ligands with amide and C=O groups oriented in an antiparallel manner (*trans*-conformation) to yield a neutral two-dimensional (2D) double-edged zinc(II)–organic 4^4-**sql** layer network (Fig. 1b),[15] with nanosized mesh of 10.06 × 20.11 $Å^2$. These 2D layers are stacked offset in an ABAB fashion along the crystallographic [010] direction (Fig. 1c). The open channels thus formed in two different window sizes with effective dimensions of approximately 2 × 4 and 4 × 9 $Å^2$, respectively. The lattice DMF and H_2O molecules are located within the open channels (Fig. S3a), occupying an extra-framework volume of approximately 28%.[16] The bis-amide groups of the coordinated bpda ligands participate in multiple hydrogen-bonding interactions. The whole crystal

structure is stabilized by moderate N−H···O hydrogen-bonding interactions among the offset-stacked layers (Fig. 1d and S3b); these net-to-net hydrogen bonds are located between the amide hydrogens of the bpda ligands in one layer and the carboxyl oxygens of the 1,3-bdc^{2-} ligands in neighbouring layers (N···O = 2.88 and 2.90 Å, Table S2). In addition, the amide groups of the bpda ligands also interact with the lattice DMF and H_2O molecules through net-to-guest N−H···O hydrogen bonds (N···O = 2.90−3.02Å, Table S2).

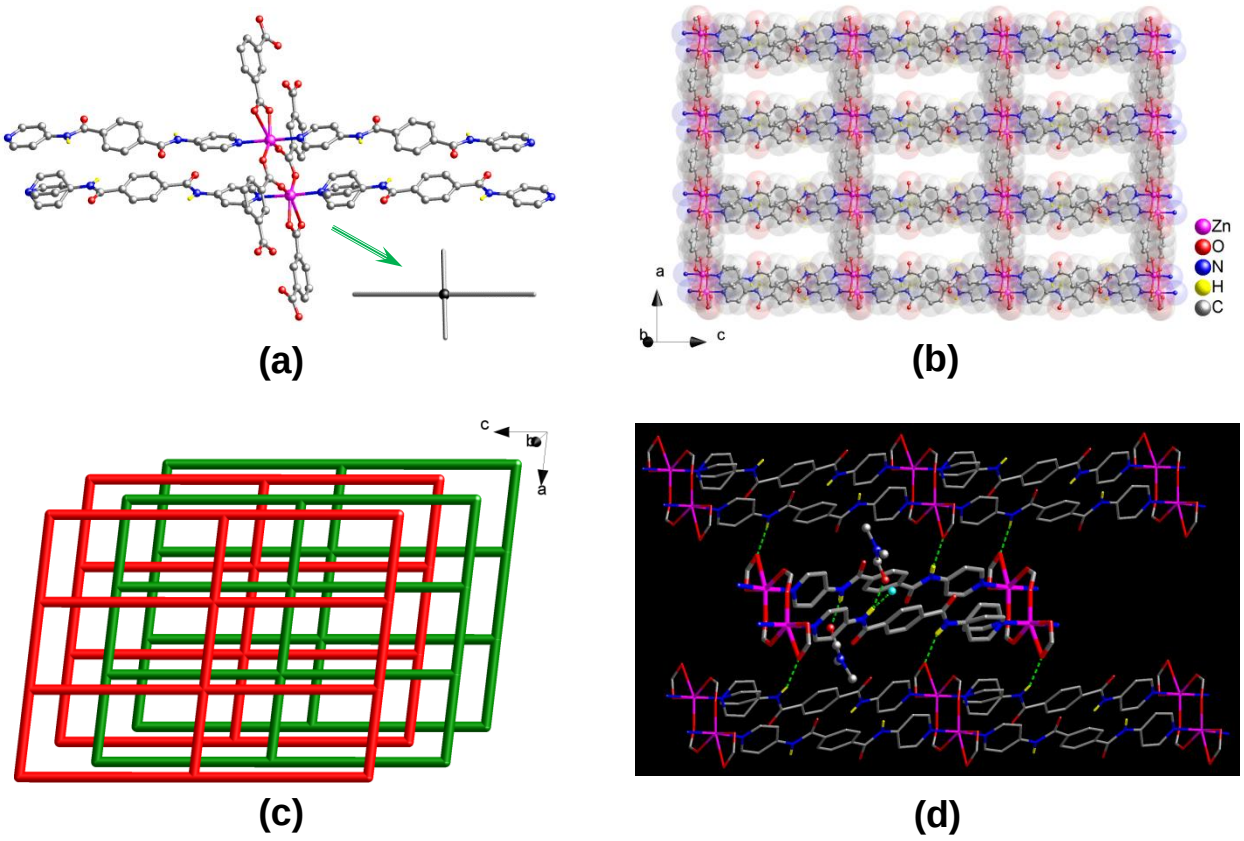

Fig. 1 Crystal structure of **1**: (a) view of a two-blade paddlewheel-like $[Zn_2(CO_2)_4N_4]$ cluster as a 4-connected node; (b) view of the 2D double-edged layer structure; (c) topologic view of the packing of the 4^4-**sql** layers along slight off the crystallographic [010] direction, showing an ABAB offset-stacking fashion; (d) highlighting the N−H···O hydrogen-bonding interactions.

[Zn_2(1,4-ndc)$(dmc)_2(bpda)_2$] (2)

A single-crystal X-ray diffraction analysis revealed that **2** crystallizes in the monoclinic space group $P2_1/c$. The asymmetric unit consists of one Zn(II) center and half of one 1,4-ndc^{2-}, one dmc^-, and one bpda ligands, where Hdmc = dimethylcarbamic acid. The dmc^- ligand is in situ generated via the hydrolysis of the DMF solvent under the hydro(solvo)thermal conditions used. The Zn(II) center adopts a five-coordinated {ZnN_2O_3} trigonal bipyramidal geometry (Fig. 2a), surrounded by two pyridine nitrogens of two different bpda ligands at the axial positions and three carboxyl oxygens of one 1,4-ndc^{2-} and two different dmc^- ligands at the equatorial plane (τ = 0.78).[14] The Zn−N bond lengths are in the range of 2.151(2)−2.154(2) Å, and the Zn−O bond lengths are in the range of 1.981(2)−2.108(2) Å. Each 1,4-ndc^{2-} ligand bridges two Zn(II) centers with the carboxyl group in a monodentate coordination mode. The remaining carboxylic oxygen is also in weak contact with the Zn(II) center (Zn···O, 2.723 Å). Each dmc^- ligand adopts a μ_2-η^1:η^1-bridging bidentate coordination mode to bridge two Zn(II) centers.

Two Zn centers are bridged by two dmc^- ligands to form a two-blade paddlewheel-like dinuclear [$Zn_2(CO_2)_4N_4$] cluster SBU, with a Zn···Zn separation of 3.95 Å (Fig. 2a). These dinuclear SBUs are stringed by the 1,4-ndc^{2-} ligands to generate a neutral 1D chain array of Zn_2(1,4-ndc)$(dmc)_2$, which is linked by pairs of bpda ligands showing a *trans*-conformation to yield a neutral 2D zinc(II)–organic 4^4-**sql** layer network (Fig. 2b),[15] with nanosized mesh of 15.06 × 20.06 $Å^2$. These 2D layers are stacked in an offset ABA′B′ fashion along the crystallographic [101] direction (Fig. 2c), causing a loss of potential openings with negligible solvent accessible volume (~0%).[16] This is comparable with the ABAB stacking arrangement in **1** that resulted in the formation of open channels. Among these offset-stacked layers, moderate net-to-net N−H···O hydrogen-bonding interactions (N···O = 2.88 and 3.03 Å, Table S2) formed between the amide hydrogens of the bpda ligands and the carboxyl oxygens of the 1,4-ndc^{2-} ligands provide clear support for stabilizing the overall crystal structure of **2** (Fig. 2d and S4).

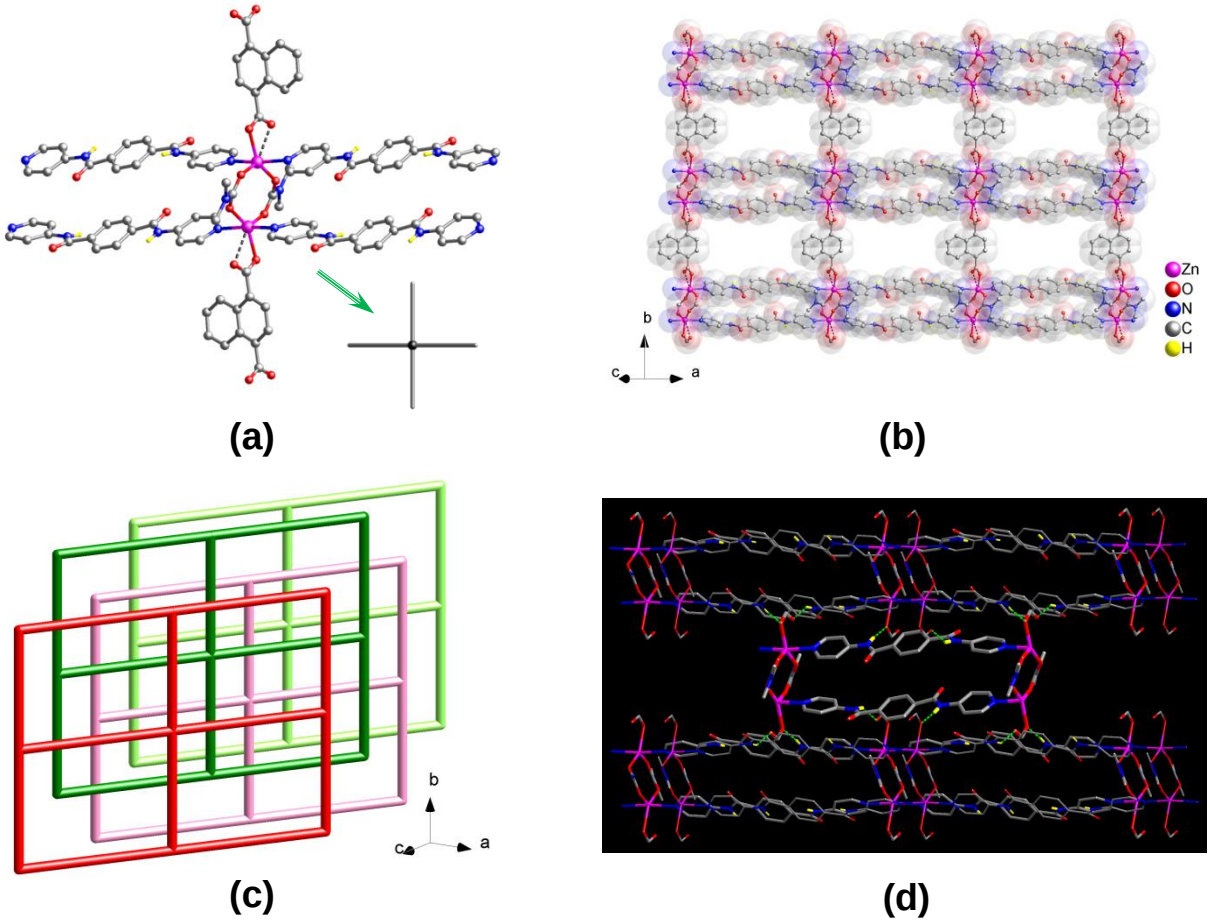

Fig. 2 Crystal structure of **2**: (a) view of a two-blade paddlewheel-like $[Zn_2(CO_2)_4N_4]$ cluster as a 4-connected node; (b) view of the 2D layer structure; (c) topologic view of the packing of the 4^4-**sql** layers along slight off the crystallographic [101] direction, showing an ABA′B′ offset-stacking fashion; (d) highlighting the net-to-net N−H···O hydrogen-bonding interactions.

Thermogravimetric properties

The thermal stabilities of compounds **1** and **2** were examined by thermogravimetric (TG) analysis, which was performed on polycrystalline samples under a nitrogen atmosphere (Fig. 3). The TG curve for **1** reveals a weight loss of 16.7% between 30 and 270 ℃, corresponding to the loss of guest H_2O and DMF molecules (calcd. 17.2%). The de-solvated sample then remained stable at temperatures up to ~335 ℃ without any weight loss and then began to decompose. The TG trace of **2** shows no significant weight loss prior to its decomposition at a temperature approaching 320 ℃. The decomposition process was complete at a temperature of about 815 ℃, leaving a final residue of 14.1% that can reasonably be assumed to be ZnO (calcd. 14.1%).

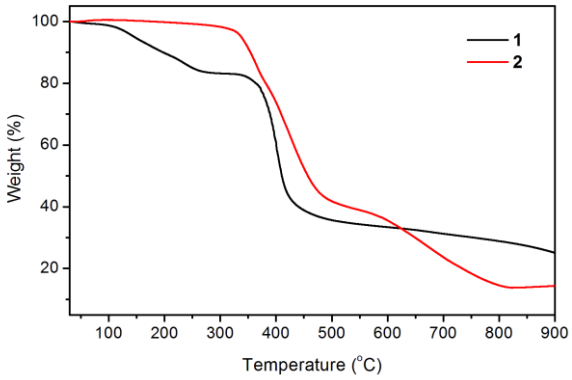

Fig. 3 Thermogravimetric (TG) curves of compounds **1** (black line) and **2** (red line).

Photoluminescence properties

The luminescence properties of compounds **1** and **2** were investigated in the solid state at room temperature, together with the free bpda, 1,3-H_2bdc, and 1,4-H_2ndc ligands (Fig. 4). Representative photoluminescence emission bands at 493 (λ_{ex} = 276 nm), 358 (λ_{ex} = 274 nm), and 476 nm (λ_{ex} = 274 nm) were observed for the free bpda, 1,3-H_2bdc, and 1,4-H_2ndc, respectively. The emissions of the organic ligands may be ascribed to $\pi^* \rightarrow$ n or $\pi^* \rightarrow \pi$ transitions.[17]

Compound **1** displays an emission band with a maximum at 426 nm upon excitation at 276 nm, whereas compound **2** emits at 414 nm (λ_{ex} = 345 nm). Based on the band position and shape, it appears that the emissions for both compounds originated from the ligand-to-metal charge transfer (LMCT) transition from carboxylate groups to Zn(II) ions, which may be admixed with a ligand-to-ligand charge transfer (LLCT), as has been observed in other Zn(II) complexes with the d^{10} valence electron configuration.[17,18]

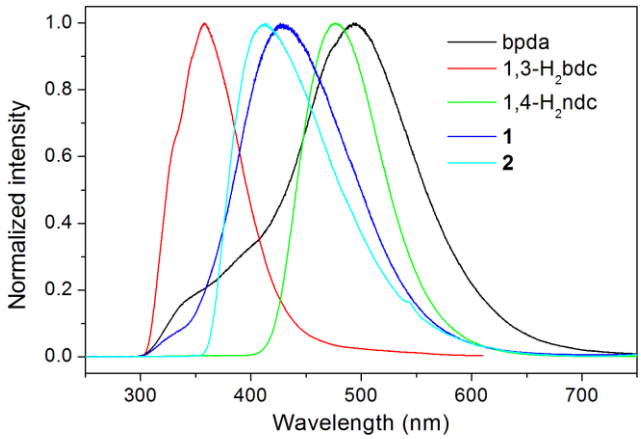

Fig. 4 Room temperature, solid-state emission spectra of the free organic ligands and compounds **1** and **2**.

CO_2 sorption

Prior to the gas adsorption experiments, we prepared a desolvated smaple of **1**, hereafter denoted as **1′**, in which guest solvent molecules in the framework had been removed. In addition, compound **2** was thermally activated, labeled as **2′**, by heating the as-synthesized sample at 120 °C for 24 h. Sorption studies showed that compounds **1′** and **2′** both exhibit moderate or low CO_2 uptake capacities at 1 atm and controlled temperatures (195, 273, and 298 K) with a reversible type I isotherm (Fig. 5), which is characteristic of microporous materials. The estimated apparent Langmuir and Brunauer−Emmett−Teller (BET) surface areas were determined to be 85 $m^2\ g^{-1}$ and 59 $m^2\ g^{-1}$, respectively, for **1′** and 122 $m^2\ g^{-1}$ and 82 $m^2\ g^{-1}$, respectively, for **2′**. Compound **1′** takes up only a small amount (1.35 mmol g^{-1}) of CO_2 at 195 K, 1.10 mmol g^{-1} of CO_2 at 273 K and 1.00 mmol g^{-1} of CO_2 at 298 K, whereas **2′** takes up 1.62, 1.24, and 0.99 mmol g^{-1} of CO_2 at 195 K, 273 K and 298 K, respectively. In comparison with some 2D layered networks, such as [Zn($5NO_2$-ip)(bpy)] ($5NO_2$-ip = 5-nitroisophthalate, bpy = 4,4′-bipyridine; 2.54 mmol g^{-1} of CO_2 at 273 K),[19] and $[\{NiL^1\}_3(BTC)_2]$ (L^1 = 3,10-bis(4-fluorobenzyl)-1,3,5,8,10,12-hexaazacyclotetradecane, BTC = 1,3,5-benzenetricarboxylate; 2.66 mmol g^{-1} of CO_2 at 273 K),[20] Both **1′** and **2′** showed low CO_2 adsorption, which may be due to the poor porosity of both frameworks and a decrease in the amount of appropriate intermolecular interactions. Furthermore, the framework of **2**, after thermal activation, may be transformed into a new phase, which is likely to be porous due to layer slip from off-stacking, as evidenced by the PXRD pattern (Fig. S2, SI) and the moderate CO_2 adsorption capability (Table 1).

The isosteric heat of CO_2 adsorption was calculated by the virial method,[7a,23] which displays commonly decreased Q_{st} traces for **1′** and **2′** with increasing CO_2 uptake (Fig. 6), depending on the amount of adsorbed CO_2 molecules. This is much different from a related report for compound $\{[Zn_4(1,4\text{-bdc})_4(bpda)_4]\cdot 5DMF\cdot 3H_2O\}_n$ (**3**), the desolvated sample (**3**') of which displayed an abnormally increased trace arising (30.2–37.2 KJ mol^{-1}) from significant cooperative effect of amide

groups in capturing CO_2.[11] Surprisingly, compound **1′** at zero coverage exhibits a weak (15.9 kJ mol^{-1}) CO_2 binding affinity, which is close to the enthalpy of liquefaction of CO_2 (17 kJ mol^{-1}), indicating that the framework surface does not provide an improvement over the affinity of the gas for itself.[24] For **2′**, although the Q_{st} value of 26.2 kJ mol^{-1} is much lower than 30.2 kJ mol^{-1} for **3'** and 36.5 kJ mol^{-1} for $[Cu_3L_2(H_2O)_5]$·Guest (where H_3L = 5-(4-carboxybenzoylamino) isophthalic acid),[11,25] it is still comparable to that of $[Cu_{24}(TPBTM^{6-})_8(H_2O)_{24}]$ (26.3 kJ mol^{-1}),[26] $Cu_3(BTB^{6-})$ (24.1 kJ mol^{-1}), and $Cu_3(TATB^{6-})$ (24.4 kJ mol^{-1}).[27]

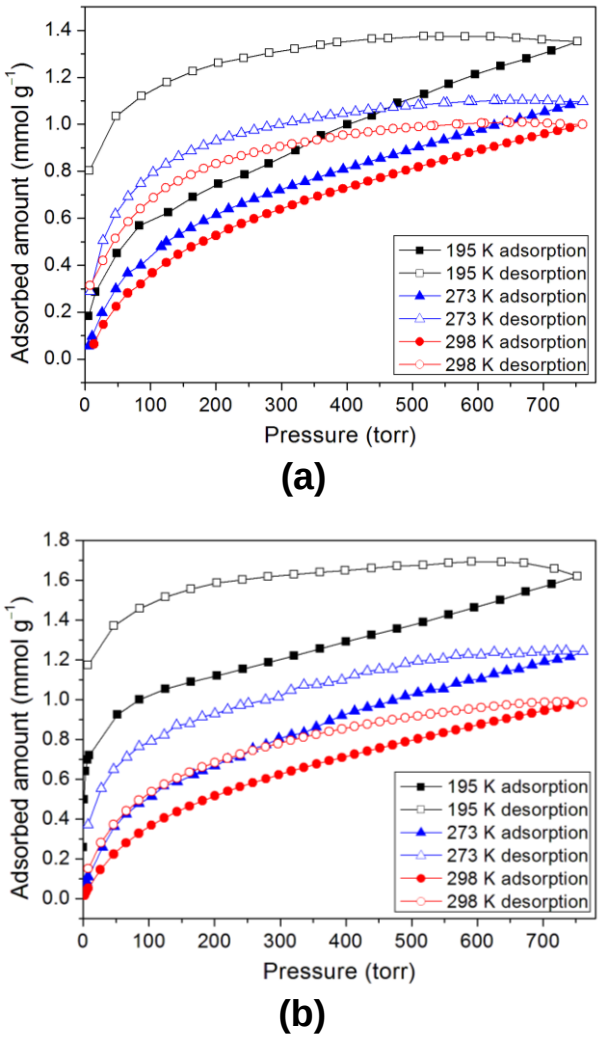

Fig. 5 Low-pressure CO_2 isotherms of (a) **1′** and (b) **2′** measured at 195 K, 273 K, and 298 K.

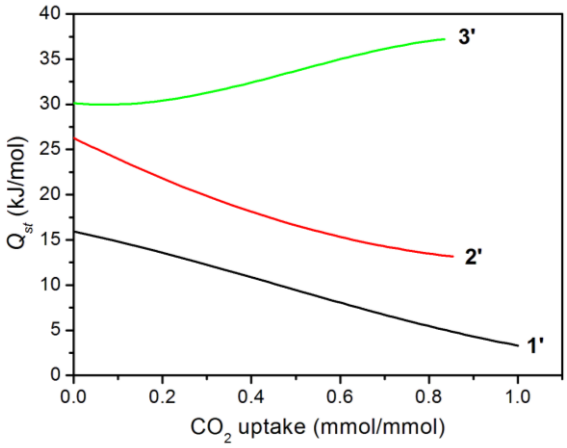

Fig. 6 Isosteric heat (Q_{st}) of CO_2 adsorption.

Structure–CO_2 capture relationship

Understanding the interrelationship between the structural characteristics of porous hosts and their CO_2 adsorption capabilities is essential for the development of new materials for use in the capture and storage of CO_2. In addition to amine-mediated MOFs, amide-mediated MOFs have also emerged as potential candidates for effectively capturing CO_2.[11,26] In this work, the most interesting observation is that the CO_2 adsorption behavior of the amide-containing Zn(II)-based MOF **1** and **2** is completely different from that of a related species **3**. A detailed comparison was therefore made to illustrate their interrelationship. As can be seen from Scheme 1, the aromatic dicarboxylate ligands (1,3-bdc, 1,4-ndc, and 1,4-bdc, respectively) of **1–3** are quite similar. Interestingly, minor variation of the ligand structures from 1,4-bdc (smaller spacer, linear ligating orientation) to 1,3-bdc (smaller spacer, angular ligating orientation) and 1,4-ndc (larger bulky spacer, linear ligating orientation), the crystal structures of **1**–**3** were drastically changed from a two-fold interpenetrated pillared-layer framework (**3**) to noninterpenetrated 2D **sql** layers (**1** and **2**), even though they were constructed from very similar two-blade paddlewheel SBUs. More important, this change results in a significant effect on the CO_2 adsorption ability of the frameworks (Table 1). For **3**, the amide groups are exposed in the large channel openings of a two-fold interpenetrated framework, permitting a significant level of cooperative binding of CO_2 in an amide:CO_2 manner and even in an amide:CO_2:CO_2 manner.[11] These

findings help to explain the observed increase in Q_{st} from a low to a 1:1 CO_2 uptake. On the other hand, both layered structures **1** and **2** show compact stacking, in which all of the amide groups are sheltered and contribute to hydrogen bonds. Therefore, it is reasonable that no meaningful cooperative binding, even primary amide:CO_2 interactions, between the amide groups and CO_2 molecules occurs in the condensed 2D structures. Weak Q_{st} values that would not increase with increasing CO_2 uptake are estimated. As a consequence, the three amide-mediated zine(II) MOF **1–3** represent an excellent example to demonstrate the intimate interrelationships between CO_2 adsorption capability and the structural characteristics of their host materials.

Table 1 Comparisons of the structural characteristics and CO_2 adsorption properties of compounds **1**−**3**[a]

	1	**2**	**3**
Dicarboxylate ligand	1,3-bdc	1,4-ndc	1,4-bdc
Frameworks	2D **sql** layer with ABAB stacking	2D **sql** layer with ABA′B′ stacking	3D 2-fold interpenetrated pillared-layer framework
Amide groups expose to channels	No	No	Yes
Solvent accessible voids (%)	28	~0	29
Langmuir surface area ($m^2\ g^{-1}$)	85	122	468
BET surface area ($m^2\ g^{-1}$)	59	82	331
CO_2 adsorption amount (195, 273, 298 K) (mmol g^{-1})	1.35, 1.10, 1.00	1.62, 1.24, 0.99	5.54, 2.83, 1.87
Q_{st} (kJ mol^{-1})	15.9−3.3	26.3−13.2	30.2−37.2
Amide:CO_2 interaction	No	No	Yes
Amide:CO_2:CO_2 interaction	No	No	Yes

Conclusion

Three amide-mediated Zn(II) MOF were synthesized from related aromatic dicarboxylate bridging ligands, i.e. from 1,4-bdc to 1,3-bdc and 1,4-ndc. An intimate interrelationship between their structural characteristics and CO_2 adsorption behavior is unambiguously demonstrated. The arrangement of the amide group in the framework determines whether or not amide:CO_2 (cooperative) interaction occurs which plays a key role in influencing the extent of CO_2 sorption. This unique ease

indeed adds to our understanding of CO_2 capture and the design of the porous host materials for achieving this.

Acknowledgments

We are grateful to the Academia Sinica and the Ministry of Science and Technology, Taiwan, for financial support.

Notes and references

1 (*a*) H. Furukawa, K. E. Cordova, M. O'Keeffe and O. M. Yaghi, *Science*, 2013, **341**, 1230444; (*b*) K. Sumida, D. L. Rogow, J. A. Mason, T. M. McDonald, E. D. Bloch, Z. R. Herm, T.-H. Bae and J. R. Long, *Chem. Rev.*, 2012, **112**, 724–781; (*c*) S. Ma and H. C. Zhou, *Chem. Commun.*, 2010, **46**, 44–53; (*d*) A. Shigematsu, T. Yamada and H. Kitagawa, *J. Am. Chem. Soc.*, 2012, **134**, 13145–13147; (*e*) P. Thanasekaran, T.-T. Luo, J.-Y. Wu and K.-L. Lu, *Dalton Trans.*, 2012, **41**, 5437–5453.

2 (*a*) X. M. Liu, R. B. Lin, J. P. Zhang and X. M. Chen, *Inorg. Chem.*, 2012, **51**, 5686–5692; (*b*) Q. Wang, J. Luo, Z. Zhong and A. Borgna, *Energy Environ. Sci.*, 2011, **4**, 42–55; (*c*) M. R. Kishan, J. Tian, P. K. Thallapally, C. A. Fernandez, S. J. Dalgarno, J. E. Warren, B. P. McGrail and J. L. Atwood, *Chem. Commun.*, 2010, **46**, 538–540; (*d*) R. Zou, A. I. Abdel-Fattah, H. Xu, Y. Zhao and D. D. Hickmott, *CrystEngComm*, 2010, **12**, 1337–1353.

3 (*a*) N. Yanai, K. Kitayama, Y. Hijikata, H. Sato, R. Matsuda, Y. Kubota, M. Takata, M. Mizuno, T. Uemura and S. Kitagawa, *Nat. Mater.*, 2011, **10**, 787–193; (*b*) S. Pramanik, C. Zheng, X. Zhang, T. J. Emge and J. Li, *J. Am. Chem. Soc.*, 2011, **133**, 4153–4155.

4 (*a*) K. S. Jeong, Y. B. Go, S. M. Shin, S. J. Lee, J. Kim, O. M. Yaghi and N. Jeong, *Chem. Sci.*, 2011, **2**, 877–882; (*b*) H. Lu and X. P. Zhang, *Chem. Soc. Rev.*, 2011, **40**, 1899–1909; (*c*) L.

Chen, Y. Yang, Z. Guo and D. Jiang, *Adv. Mater.*, 2011, **23**, 3149–3154; (*d*) L. Ma, J. M. Falkowski, C. Abney and W. Lin, *Nature Chem.*, 2010, **2**, 838–846.

5 (*a*) R. C. Huxford, J. Della Rocca and W. Lin, *Curr. Opin. Chem. Biol.*, 2010, **14**, 262–268; (*b*) P. Horcajada, T. Chalati, C. Serre, B. Gillet, C. Sebrie, T. Baati, J. F. Eubank, D. Heurtaux, P. Clayette, C. Kreuz, J. S. Chang, Y. K. Hwang, V. Marsaud, P. N. Bories, L. Cynober, S. Gil, G. Férey, P. Couvreur and R. Gref, *Nat. Mater.*, 2009, **9**, 172–178.

6 (*a*) T. Devic, P. Horcajada, C. Serre, F. Salles, G. Maurin, B. Moulin, D. Heurtaux, G. Clet, A. Vimont, J. M. Greneche, B. Le Ouay, F. Moreau, E. Magnier, Y. Filinchuk, J. Marrot, J. C. Lavalley, M. Daturi and G. Férey, *J. Am. Chem. Soc.*, 2010, **132**, 1127–1136; (*b*) R. M. P. Colodrero, P. Olivera-Pastor, E. R. Losilla, D. Hernandez-Alonso, M. A. G. Aranda, L. Leon-Reina, J. Rius, K. D. Demadis, B. Moreau, D. Villemin, M. Palomino, F. Rey and A. Cabeza, *Inorg. Chem.*, 2012, **51**, 7689–7698.

7 (*a*) Y.-S. Bae and R. Q. Snurr, *Angew. Chem. Int. Ed.*, 2011, **50**, 11586–11596; (*b*) D. M. D'Alessandro, B. Smit and J. R. Long, *Angew. Chem., Int. Ed.*, 2010, **49**, 6058–6082; (*c*) T. Düren, Y.-S. Bae and R. Q. Snurr, *Chem. Soc. Rev.*, 2009, **38**, 1237–1247; (*d*) A. R. Millward and O. M. Yaghi, *J. Am. Chem. Soc.*, 2005, **127**, 17998–17999.

8 (*a*) A. M. Fracaroli, H. Furukawa, M. Suzuki, M. Dodd, S. Okajima, F. Gándara, J. A. Reimer and O. M. Yaghi, *J. Am. Chem. Soc.*, 2014, **136**, 8863–8866; (*b*) R. Vaidhyanathan, S. S. Iremonger, G. K. H. Shimizu, P. G. Boyd, S. Alavi and T. K. Woo, *Science*, 2010, **330**, 650–653; (*c*) R. Vaidhyanathan, S. S. Iremonger, K. W. Dawson and G. K. H. Shimizu, *Chem. Commun.*, 2009, 5230–5232; (*d*) J. An, S. J. Geib and N. L. Rosi, *J. Am. Chem. Soc.*, 2010, **132**, 38–39; (*e*) A. Demessence, D. M. D'Alessandro, M. L. Foo and J. R. Long, *J. Am. Chem. Soc.*, 2009, **131**, 8784–8786; (*f*) S. Couck, J. F. M. Denayer, G. V. Baron, T. Remy, J. Gascon and F. Kapteijn, *J. Am. Chem. Soc.*, 2009, **131**, 6326–6327; (*g*) B. Arstad, H. Fjellvåg, K. O. Kongshaug, O. Swang and R. Blom, *Adsorption*, 2008, **14**, 755–762.

9 (*a*) S. S. Mondal, A. Bhunia, I. A. Baburin, C. Jäger, A. Kelling, U. Schilde, G. Seifert, C. Janiak and H.-J. Holdt, *Chem. Commun.*, 2013, **49**, 7599–7601; (*b*) F. Debatin, A. Thomas, A. Kelling, N. Hedin, Z. Bacsik, I. Senkovska, S. Kaskel, M. Junginger, H. Müller, U. Schilde, C. Jäger, A. Friedrich and H.-J. Holdt, *Angew. Chem., Int. Ed.*, 2010, **49**, 1258–1262; (*c*) Y. Zhao, H. Wu, T. J. Emge, Q. Gong, N. Nijem, Y. J. Chabal, L. Kong, D. C. Langreth, H. Liu, H. Zeng and J. Li, *Chem.—Eur. J.*, 2011, **17**, 5101–5109; (*d*) E. Neofotistou, C. D. Malliakas and P. N. Trikalitis, *Chem.—Eur. J.*, 2009, **15**, 4523–4527.

10 (*a*) B. Zheng, Z. Yang, J. Bai, Y. Li and S. Li, *Chem. Commun.*, 2012, **48**, 7025–7027; (*b*) J. Duan, Z. Yang, J. Bai, B. Zheng, Y. Li and S. Li, *Chem. Commun.*, 2012, **48**, 3058–3060; (*c*) B. Zheng, J. Bai, J. Duan, L. Wojtas and M. J. Zaworotko, *J. Am. Chem. Soc.*, 2011, **133**, 748–751; (*d*) B. Zheng, H. Liu, Z. Wang, X. Yu, P. Yia and J. Bai, *CrystEngComm*, 2013, **15**, 3517–3520; (*e*) C. Hou, Q. Liu, T. Okamura, P. Wang and W.-Y. Sun, *CrystEngComm*, 2012, **14**, 8569–8576; (*f*) M.-J. Sie, Y.-J. Chang, P.-W. Cheng, P.-T. Kuo, C.-W. Yeh, C.-F. Cheng, J.-D. Chen and J.-C. Wang, *CrystEngComm*, 2012, **14**, 5505–5516.

11 C.-H. Lee, H.-Y. Huang, Y.-H. Liu, T.-T. Luo, G.-H. Lee, S.-M. Peng, J.-C. Jiang, I. Chao and K.-L. Lu, *Inorg. Chem.*, 2013, **52**, 3962−3968.

12 C.-H. Lee, J.-Y. Wu, G.-H. Lee, S.-M. Peng, J.-C. Jiang and K.-L. Lu, *Cryst. Growth Des.*, 2014, **14**, 5608–5616.

13 G. M. Sheldrick, *SHELX-97* (including *SHELXS* and *SHELXL*); University of Göttingen: Göttingen, Germany, 1997.

14 A. W. Addison, T. N. Rao, J. Reedijk, J. van Rijn and G. C. Verschoor, *J. Chem. Soc., Dalton Trans.*, 1984, 1349–1356.

15 For the three-letter net codes, see (*a*) M. O'Keeffe, M. A. Peskov, S. J. Ramsden and O. M. Yaghi, *Acc. Chem. Res.*, 2008, **41**, 1782−1789; (*b*) N. W. Ockwig, O. Delgado-Friedrichs, M. O'Keeffe

and O. M. Yaghi, *Acc. Chem. Res.*, 2005, **38**, 176−182; (*c*) The associated website, http://rcsr.anu.edu.au/home.

16 *PLATON*: A. L. Spek, *J. Appl. Crystallogr.*, 2003, **36**, 7–13.

17 W. Chen, J.-Y. Wang, C. Chen, Q. Y.-M. Yuan, J.-S. Chen and S.-N. Wang, *Inorg. Chem.*, 2003, **42**, 944–946.

18 (*a*) M. D. Allendorf, C. A. Bauer, R. K. Bhakta and R. J. T. Houk, *Chem. Soc. Rev.*, 2009, **38**, 1330–1352; (*b*) J.-Y. Wu, P.-T. Yuan and C.-C. Hsiao, *CrystEngComm*, 2014, **16**, 3128–3140; (*c*) C. Y. Xu, Q. Q. Guo, X. J. Wang, H. W. Hou and Y. T. Fan, *Cryst. Growth Des.*, 2011, **11**, 1869–1879; (*d*) M. Du, X.-J. Jiang and X.-J. Zhao, *Inorg. Chem.*, 2007, **46**, 3984–3995; (*e*) Q. Chu, G.-X. Liu, Y.-Q. Huang, X.-F. Wang and W.-Y. Sun, *Dalton Trans.*, 2007, 4302–4311; (*f*) S.-L. Zheng, J.-H. Yang, X.-L. Yu, X.-M. Chen and W.-T. Wong, *Inorg. Chem.*, 2004, **43**, 830–838.

19 S. Horike, Y. Inubushi, T. Hori, T. Fukushima and S. Kitagawa, *Chem. Sci.*, 2012, **3**, 116–120.

20 Y. Inubushi, S. Horike, T. Fukushima, G. Akiyama, R. Matsuda and S. Kitagawa, *Chem. Commun.*, 2010, **46**, 9229–9231.

21 J. L. C. Rowsell and O. M. Yaghi, *J. Am. Chem. Soc.*, 2006, **128**, 1304−1315.

22 A. Demessence, D. M. D'Alessandro, M. L. Foo and J. R. Long, *J. Am. Chem. Soc.*, 2009, **131**, 8784–8786.

23 J. Duan, Z. Yang, J. Bai, B. Zheng, Y. Li and S. Li, *Chem. Commun.*, 2012, **48**, 3058−3060.

24 B. Zheng, J. Bai, J. Duan, L. Wojtas and M. J. Zaworotko, *J. Am. Chem. Soc.*, 2011, **133**, 748−751.

25 B. Zheng, Z. Yang, J. Bai, Y. Li and S. Li, *Chem. Commun.*, 2012, **48**, 7025−7027.

26 (*a*) Zheng, B.; Bai, J.; Duan, J.; Wojtas, L.; Zaworotko, M. J. *J. Am. Chem. Soc.*, 2011, **133**, 748–751. (b) Tzeng, B.-C.; Chiu, T.-H.; Chen, B.-S.; Lee, G.-H. *Chem. Eur. J.*, 2008, **14**, 5237–5245. (c) Hasegawa, S.; Horike, S.; Matsuda, R.; Furukawa, S.; Mochizuki, K.; Kinoshita, Y.; Kitagawa, S. *J. Am. Chem. Soc.*, 2007, **129**, 2607–2614. (d) Adarsh, N. N.; Kumar, D. K.; Dastidar, P. *CrystEngComm*, 2009, **11**, 796–802. (e) Song, X.; Zou, Y.; Liu, X.; Oha, M.; Lah, M. S. *New J. Chem.*, 2010, **34**, 2396–2399. (f) Duan, J.; Yang, Z.; Bai, J.; Zheng, B.; Lia, Y.; Li,

S. *Chem. Commun.*, 2012, **48**, 3058–3060. (g) Zheng, B.; Yang, Z.; Bai, J.; Lia, Y.; Li, S. *Chem. Commun.*, 2012, **48**, 7025–7027.

Graphical contents entry

Amide-containing zinc(II) metal–organic layer networks: structure–CO_2 capture relationship

Cheng-Hua Lee,[ab] Jing-Yun Wu,*[c] Gene-Hsiang Lee,[d] Shie-Ming Peng,[d] Jyh-Chiang Jiang,[e] and Kuang-Lieh Lu*[a]

[a]*Institute of Chemistry, Academia Sinica, Taipei 115, Taiwan. Fax: +886-2-27831237; E-mail: kllu@gate.sinica.edu.tw*
[b]*Graduate Institute of Applied Science and Technology, National Taiwan University of Science and Technology, Taipei 106, Taiwan*
[c]*Department of Applied Chemistry, National Chi Nan University, Nantou 545, Taiwan. E-mail: jyunwu@ncnu.edu.tw*
[d]*Department of Chemistry, National Taiwan University, Taipei 107, Taiwan*
[e]*Department of Chemical Engineering, National Taiwan University of Science and Technology, Taipei 106, Taiwan*

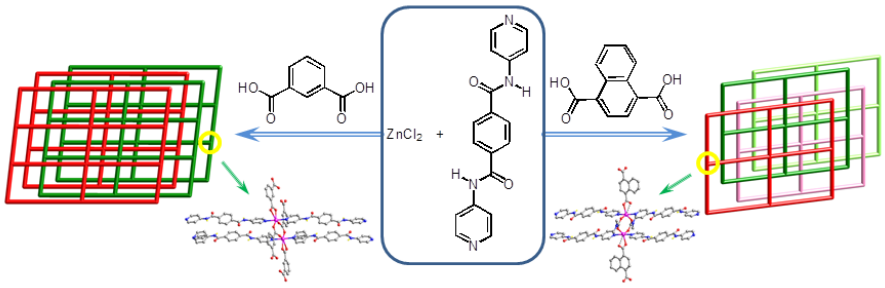

An intimate interrelationship between the structural characteristics and their CO_2 adsorption behavior has been demonstrated from this study.